Energy & Environmental Science

Building a stable cationic molecule/electrode interface for highly efficient and durable CO2 reduction at an industrial-relevance current

Journal:	*Energy & Environmental Science*
Manuscript ID	EE-ART-08-2020-002535.R2
Article Type:	Paper
Date Submitted by the Author:	24-Nov-2020
Complete List of Authors:	Su, Jianjun; City University of Hong Kong Zhang, Jun-Jie; Rice University Chen, Jiacheng; East China University of Science and Technology Song, Yun; City University of Hong Kong Huang, Libei; City University of Hong Kong Zhu, Minghui; East China University of Science and Technology, Chemical Engineering Yakobson, Boris; Rice University, Tang, Ben Zhong; The Hong Kong University of Science and Technology, Department of Chemistry Ye, Ruquan; City University of Hong Kong College of Science and Engineering,

ARTICLE

Building a stable cationic molecule/electrode interface for highly efficient and durable CO_2 reduction at an industrial-relevance current

Received 00th January 20xx,
Accepted 00th January 20xx

DOI: 10.1039/x0xx00000x

Jianjun Su,[a] Jun-Jie Zhang,[b] Jiacheng Chen,[c] Yun Song,[a] Libei Huang,[a] Minghui Zhu,*[c] Boris I. Yakobson,[b] Benzhong Tang[d,e,f] and Ruquan Ye*[a,g]

Aggregation and leaching are two major obstacles to the synthesis of efficient and durable heterogeneous molecular catalysts. These problems are even more severe for charged molecules, which not only result in unsatisfactory performance, but also lead to a misleading evaluation of charged functionalities. In this work, methylation of cobalt (II) tetraamino phthalocyanine (CoTAPc) transforms the electron-donating amino groups into electron-withdrawing quaternary ammonium cations, which favor the formation of *COOH intermediate and the desorption of *CO, conducive to 130% increase of current density for CO_2 reduction reaction (CO_2RR). However, the catalysts leach severely and consequently the current density decays rapidly. To resolve the dilemma, we develop an in situ functionalization strategy by first covalently grafting CoTAPc onto carbon nanotube via a diazo-reaction, followed by a complete methylation reaction. This conduces to 700% increase in CO partial current density compared to that of physically mixed sample at -0.72 V vs. RHE with highly stable currents. In a flow cell, this covalently immobilized structure delivers an industrial-relevance current density of 239 mA/cm^2, CO selectivity of 95.6 % at 590 mV overpotential and a very low molecular loading of 0.069 mg/cm^2. This work provides mechanistic insight and design strategy of charged molecular catalysts for high-performance and stable heterogeneous electrolysis.

Introduction

Electrochemical reduction of carbon dioxide (CO_2) using renewable electricity is an effective process for the production of useful fuel and chemical commodities.[1,2] This attractive process could not only mitigate the global warming by fixing CO_2, but also provide a pathway to store electricity into chemical energy.[3,4] Many efforts have been devoted to achieving efficient electrochemical CO_2 reduction reaction (CO_2RR) with high activity, selectivity and stability at low overpotential.[5,6] Among numerous, molecular complexes for the production of CO have attracted significant research attention as CO is an important precursor for diverse commodity chemicals synthesized by the Fischer–Tropsch process.[7,8] One advantage of molecular catalysts lies in their well-defined active sites and tunable property, which will be conducive to the understanding of structure-activity relationships and the rational design of high-performance catalysts.[9,10]

Peripheral functionalization with different substituents has been proved to be an effective method to enhance the electrocatalytic performance of molecular catalysts.[11,12] The functional groups can tune the electronic properties of metal center by inductive effect. For example, cobalt phthalocyanine with eight cyano substituents $CoPc(CN)_8$ shows a higher activity and selectivity than CoPc by facilitating the formation of active sites Co(I) and the CO desorption.[13] In our previous work, electron-donating groups on cobalt tetraphenylporphyrin (CoTPP) were found to improve the CO_2RR by increasing the electron density of the cobalt center and promoting the electrosorption of CO_2.[14] Another effect of peripheral functionalities is the electrostatic interactions. It was suggested that cationic groups favor the formation of intermediate in the rate-determining step by electrostatic stabilization. Both enhancements have been observed on CoPc and CoTPP with quaternary ammonium cation compared to their unsubstituted ones.[14,15]

Heterogenization of molecular catalysts can achieve a great improvement of current densities and stability by facilitating the charge transfer.[13,16,17] However, the existence of positive

[a] Department of Chemistry, State Key Lab of Marine Pollution, City University of Hong Kong, Hong Kong 999077, China. E-mail: ruquanye@cityu.edu.hk
[b] Department of Materials Science and Nano Engineering and Department of Chemistry, Rice University, 6100 Main Street, Houston, Texas 77005, USA.
[c] State Key Laboratory of Chemical Engineering, East China University of Science and Technology, Shanghai 200237, China. E-mail: minghuizhu@ecust.edu.cn
[d] Department of Chemistry, Hong Kong Branch of Chinese National Engineering Research Center for Tissue Restoration and Reconstruction and Institute for Advanced Study, SCUT-HKUST Joint Research Institute, The Hong Kong University of Science and Technology, Clear Water Bay, Kowloon, Hong Kong 999077, China.
[e] HKUST-Shenzhen Research Institute, No. 9 Yuexing 1st Rd, South Area, Hi-tech Park, Nanshan, Shenzhen 518057, China.
[f] Center for Aggregation-Induced Emission, State Key Laboratory of Luminescent Materials and Devices, South China University of Technology, Tianhe Qu, Guangzhou 510640, China.
[g] City University of Hong Kong Shenzhen Research Institute, Shenzhen, Guangdong 518057, China.
Electronic Supplementary Information (ESI) available: See DOI: 10.1039/x0xx00000x

charge, such as pyridinium and quaternary ammonium groups, will increase the water solubility of the molecules, resulting in poor stability.[18,19] The solubility issue might be mitigated by using an oppositely charged conductive substrate. For example, by using reduced graphene oxide (rGO) and nitrogen-doped reduced graphene oxide, both iron tetra-(4-N,N,N-trimethylanilinium)porphyrin (FeTMAP)[20] and cobalt tetra-(4-N,N,N-trimethylanilinium)porphyrin (CoTMAP)[21] can be immobilized through the π-π stacking and electrostatic interactions. These strategies improve the durability, yet the turnover frequency (TOF) values are very small. We hypothesize that the strong electrostatic interactions between the molecular catalysts and rGO result in a sandwich structure and decrease the accessibility of CO_2 to the metal center.[22,23] In addition, the hydrothermal reaction for the catalyst synthesis might decompose the quaternary ammonium groups.[21]

To this end, there is a dilemma between the stability and activity of molecular catalysts in improving its CO_2RR activity via charge engineering. Herein, combining the experimental data and theoretical prediction, we first study the cationic effect in boosting the CO_2RR of molecular catalysts. Three model samples are used, which include CoPc, cobalt (II) tetraamino phthalocyanine (CoTAPc), and cobalt (II) tetra-(4-N,N,N-trimethylanilinium) phthalocyanine (CoTMAPc). As expected, CoTMAPc shows the highest CO_2RR activity, yet the four quaternary ammonium groups significantly increase the water solubility and the current densities decay quickly. To resolve the dilemma, we covalently immobilize CoTMAPc onto carbon nanotube (CNT) through a diazo-reaction between CoTAPc and CNT, followed by a methylation reaction. This strategy conduces to a high current density of 239 mA/cm^2 and FE_{CO} of 95.6 % at -0.7 V vs. RHE with excellent stability in a flow cell configuration.

Results and discussion

Characterization and electrocatalytic performance of CoPc, CoTAPc and CoTMAPc Catalysts.

The cationically charged CoTMAPc was synthesized by methylation of CoTAPc with excess CH_3I to transform the four amino groups into quaternary ammonium cations.[24] Fig. 1a shows the chemical structure and the photos of the three molecules in water (left to right: CoPc, CoTAPc and CoTMAPc). The introduction of charged functional groups also greatly increases the water solubility (Fig. 1a). The transformation of amino group in CoTAPc into trimethylamino group of CoTMAPc was confirmed by Fourier transform infrared (FT-IR) (Fig. S1) and ^{1}H nuclear magnetic resonance (^{1}H NMR) (Fig. S2) spectroscopy. The N-H stretching peaks at 3333 and 3208 cm^{-1} of CoTAPc disappeared in CoTMAPc.[25] The prominent -CH_3 stretching vibration in -$N^+(CH_3)_3$ group at 1484 cm^{-1} and C-N bending vibration in -N^+-$(CH_3)_3$ at 944 cm^{-1} appear in CoTMAPc.[26] The ^{1}H NMR spectrum of CoTMAPc also shows a strong signal at 3.18 ppm from the methyl proton.[27] Raman spectra (Fig. S3) of CoTAPc and as-prepared CoTMAPc show a characteristic absorption peak at about 1000-1600 cm^{-1}.[28] In the UV-visible (UV-vis) spectra (Fig. S4), the Q band absorbance peak of CoTMAPc is blue-shifted to 669.8 nm after methylation, which is attributed to the strong electron withdrawing of trimethylamino group.[29] Therefore, the above characterization confirmed the successful synthesis of the positively charged CoTMAPc molecule.

The CO_2RR activity of molecular catalysts was evaluated in a home-made three-compartment cell[21,36] in CO_2-saturated 0.5 M $KHCO_3$ with a molecular loading of 7×10^{-9} mol/cm^2. The working electrode was prepared by dispersing 4.5 μmol of molecular catalysts in 10 mL DMF with 200 μL Nafion and dropping 20 μL catalyst ink on the carbon paper (0.5-inch diameter). Compared with CoPc, CoTAPc has a more negative redox potential, while CoTMAPc has a more positive redox potential in CO_2 and N_2 saturated electrolyte (Fig. S5) which further demonstrates the electron-withdrawing effect of peripheral cationic functional groups on the CoPc molecule. Linear sweep voltammetry (LSV) shows that all catalysts exhibited similar onset potentials at ~ -0.4 V vs RHE (Fig. 1b). The CO partial current densities (j_{CO}) and turnover frequency (TOF_{CO}) exhibited similar trends (Fig. S6). CoTMAPc shows much higher initial j_{CO} (1.87 mA/cm^2) and TOF (1.39 s^{-1}) at -0.72 V than those of CoPc (j_{CO} = 1.42 mA/cm^2, TOF = 1.05 s^{-1}) and CoTAPc (j_{CO} = 1.19 mA/cm^2, TOF = 0.88 s^{-1}). As depicted in Fig. 1c, the Faradaic efficiencies for CO (FE_{CO}) of these three molecules have the roughly same trend, which increases from 70 % at their onset overpotentials to 85 % at -0.57 V vs. RHE, and levels to ~87 % at potentials more negative than -0.57 V. The ~120 mV/dec Tafel slope (Fig. S7) of both three molecules indicate a one-electron transfer rate-limiting step without mass-transport limit.[30,31]

The variation of Gibbs free energy of the reaction pathway was calculated to provide mechanistic insight into the CO_2RR activity. The top and side views of CoTAPc and CoTMAPc and their intermediate steps of CO_2RR are listed in Table S1. As shown in

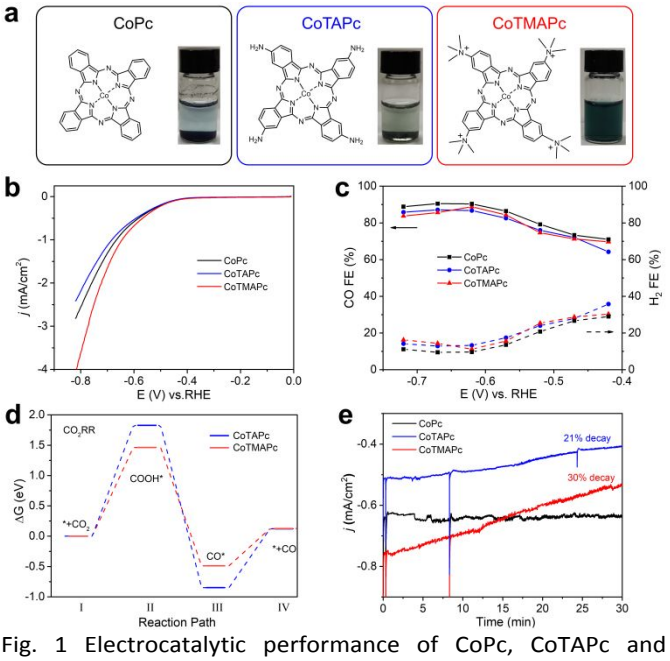

Fig. 1 Electrocatalytic performance of CoPc, CoTAPc and CoTMAPc in CO_2 saturated 0.5 M $KHCO_3$. (a) Chemical structure and photos of CoPc, CoTAPc and CoTMAPc in water (0.7 μmol/mL). (b) Linear sweep voltammograms curves at a sweep rate of 10 mV/s. (c) Faradaic efficiencies at different potentials. (d) CO_2 free energy profiles for CO_2RR to CO catalyzed by

CoTAPc and CoTMAPc and (e) Long-term electrolysis at -0.62 V versus RHE.

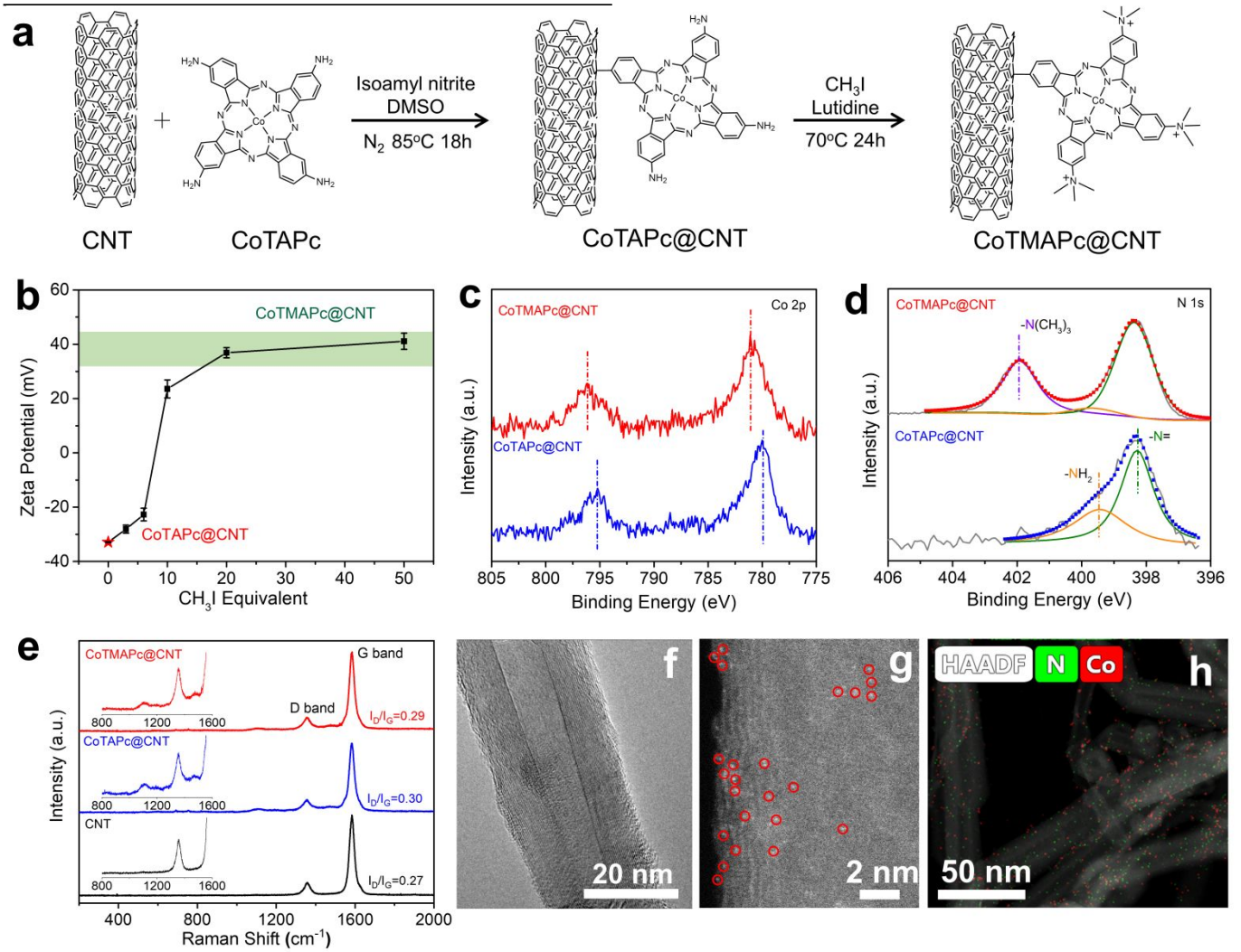

Fig. 2 Strategy for heterogenizing CoTMAPc onto CNT. (a) Scheme for the synthesis of CoTMAPc@CNT. (b) Zeta potentials of CoTMAPc@CNT as a function of CH_3I equivalent. High-resolution XPS spectra of the (c) Co 2p and (d) N 1s of CoTAPc@CNT and CoTMAPc@CNT. (e) Raman spectra of pristine CNT, CoTAPc@CNT and CoTMAPc@CNT. (f) A typical TEM image and (g) HADDF-STEM image of CoTMAPc@CNT. The circled bright spots highlight the dispersed Co centers. (h) N and Co EDS elemental mapping of CoTMAPc@CNT.

Fig. 1d, the change of variation of free energy, Δ(ΔG), for the rate-determining step (the conversion of CO_2 to *COOH, where * indicates adsorbed species)[30] is 1.46 eV on CoTMAPc, which is lower than CoTAPc by 0.37 eV. Moreover, the Δ(ΔG) for the CO desorption on CoTMAPc is only 0.62 eV, significantly lower than that of CoTAPc (0.97 eV). The variation of Gibbs free energy diagram for hydrogen evolution reaction (HER) process of CoTAPc and CoTMAP is shown in Fig. S8. The $\Delta(\Delta G_H)$ of CoTMAPc was calculated to be 0.79 eV, which is higher than that of CoTAPc (0.77 eV), indicating that HER reaction is more difficult to occur for CoTMAPc. The computation result indicates that compared to the electron-donating amino groups, the electron-withdrawing quaternary ammonium groups on CoTMAPc favor the formation of *COOH and the desorption of CO, which collectively benefit the CO_2RR to CO and is consistent with our experimental data.

However, the improved solubility of charged molecular catalysts results in very poor stability of CO_2RR performance. During the stability measurement at -0.62 V in Fig. 1e, the CoPc shows a good stability in 30 min with almost no current decrease. However, the current densities of CoTAPc and CoTMAPc samples decreased quickly by 20.9 % and 30 % after 30 min, respectively. This is because of the introduction of water-soluble amino and trimethylamino group in CoTAPc and CoTMAPc, resulting in catalysts leaching during continuous electrolysis.

Synthesis and Characterization of CoTMAPc@CNT.

In order to solve the leaching problem of CoTMAPc molecule for CO_2RR, we further developed a strategy to covalently immobilize the CoTMAPc on CNT. The CoTAPc was firstly anchored on the CNT by diazonium reaction and the amino groups were then transformed to quaternary ammonium groups by methylation reaction (Fig. 2a). To control the

selectivity, there are two important steps in the synthesis. First, the ratio of isoamyl nitrite to CoTAPc was 1:1, so that not all the four amino groups of CoTAPc were converted to diazonium. Second, the isoamyl nitrite was slowly added to the dispersed CoTAPc, so that the amino groups were in great excess. Fig. 2b shows the change of zeta potential of CoTAPc@CNT with CH_3I equivalent in methylation reaction. The zeta potential value of CoTAPc@CNT greatly increases from -22.8 mV to 20.2 mV when the CH_3I equivalent increases from 6 to 10, and then levels off at ~ 40 mV when the CH_3I equivalent further increases from 20 to 50, which suggests the complete methylation. The methylation can also be inferred from the XPS data. As shown in Fig. 2c, CoTMAPc@CNT has a Co $2p_{3/2}$ and Co $2p_{1/2}$ signal at 781.1 eV and 796.1 eV, respectively, which are higher than that of CoTAPc@CNT at 780.0 eV and 795.2 eV. The variation is due to the transformation of electron-donating amino groups into electron-withdrawing quaternary ammonium groups, leading to a decrease in the electron density of Co. Similarly, the N 1s peaks (Fig. 2d) of N atoms in phthalocyanine increase from 398.3 eV in CoTAPc@CNT to 398.4 eV in CoTMAPc@CNT.[32] Moreover, the appearance of N 1s peak at 401.9 eV in CoTMAPc@CNT further demonstrates the formation of quaternary ammonium.[33] The N:Co atomic ratios of CoTAPc@CNT and CoTMAPc@CNT from XPS (Table S2.) are 11.06 and 11.00, respectively, which suggests the tethering and functionalization occurs in accordance with figure 2a. The UV-vis spectra (Fig. S9) of CoTMAPc@CNT show an absorption peak at 684.2 nm, which slightly blue shifts compared to that of CoTAPc@CNT (687.8 nm). This trend agrees with the peak shift of molecular catalysts in Fig. S4. Additionally, the Q band absorbance peak of CoTMAPc@CNT (684.2 nm) was red-shifted when compared to that of CoTMAPc (669.8 nm), while the Q band of CoTAPc@CNT (687.8 nm) was blue-shifted to that of CoTAPc (701.7 nm). This is because the grafted molecules lose an electron-donating NH_2 group in CoTAPc@CNT and an electro

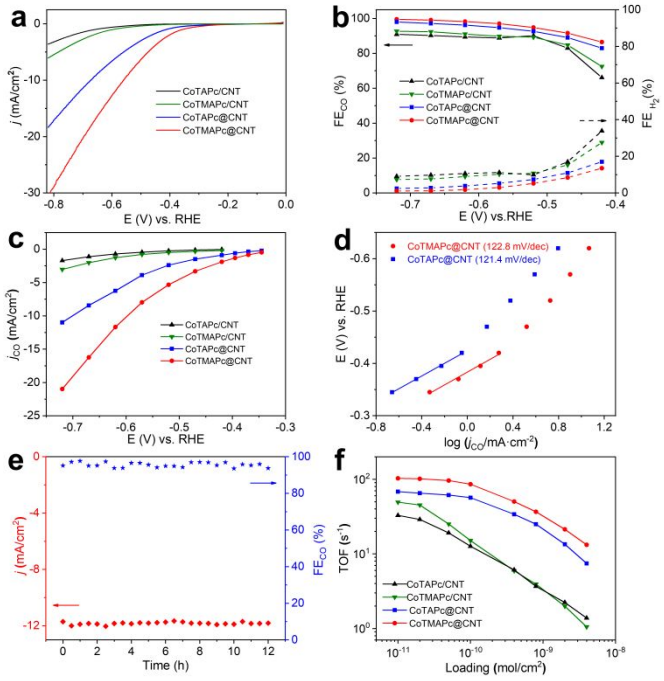

Fig. 3 CO_2RR activities of CoTAPc@CNT, CoTMAPc@CNT, CoTAPc/CNT and CoTMAPc/CNT in CO_2 saturated 0.5 M $KHCO_3$. (a) LSV curves acquired at a scan rate of 10 mv/s. The catalyst loading is ~ 7×10^{-9} mol/cm^2. (b) FE of CO and H_2. (c) CO partial current densities. (d) Tafel slopes of CoTAPc@CNT and CoTMAPc@CNT. (e) Long-term stability of CoTMAPc@CNT at -0.62 V vs. RHE and (f) TOF_{CO} at -0.62 V with different catalyst loadings.

n-withdrawing $N^+(CH_3)_3$ group in CoTMAPc@CNT. Fig. 2e presents the Raman spectra of pristine CNT, CoTAPc@CNT and CoTMAPc@CNT. CNT has two signature peaks at 1357 and 1582 cm^{-1}, which correspond to the D and G bands. The CoTAPc@CNT and CoTMAPc@CNT exhibit some fine signals from molecular catalysts at 1000-1500 cm^{-1}.[34] The ratio of the D to G peak intensity (I_D/I_G) reflects the degree of disorder of carbon materials. The molecule modified CNT samples have a higher I_D/I_G ratio (~0.3) than pristine CNT (0.27), which likely comes from the disturbance of surface lattice after the covalent grafting.[35]

Transmission electron microscopy (TEM) reveals that CoTAPc@CNT and CoTMAPc@CNT possess a similar smooth outer surface morphology to that of pristine CNT without obvious aggregation of molecular catalysts (Fig. 2f and S10). Z-contrast high-angle annular dark field of high-resolution aberration-corrected scanning transmission electron microscopy (HADDF-STEM) image (Fig. 3g) of CoTMAPc@CNT shows the high dispersion of Co sites on CNT surface, as indicated by the circled bright spots. The energy dispersive X-ray spectroscopy (EDS) maps (Fig. 2h) also show the uniform distribution of N and Co elements alongside the CNT. Inductively coupled plasma mass spectrometry (ICP-MS) was carried out to determine the Co content in the as-prepared composite material. The Co content in CoTAPc@CNT and CoTMAPc@CNT were found approximately 0.55 wt %, corresponding to 5.7 wt% and 6.9 wt% of CoTAPc and CoTMAPc in the hybrid.

Electrocatalytic CO_2RR Performance of CoTMAPc@CNT.

The CO_2RR electrochemical performance of CoTAPc@CNT and CoTMAPc@CNT was tested with a total mass loading of 75 μg/cm^2, corresponding to a molecule catalyst loading of ~ 7×10^{-9} mol/cm^2. We also took the physically mixed samples, CoTAPc/CNT and CoTMAPc/CNT, with the same molecule catalyst loading for comparison. We first estimate the number of electrochemically active sites by measuring the cyclic voltammogram (CV) of the catalyst (Fig. S11a,c). The surface-active Co sites of CoTAPc@CNT and CoTMAPc@CNT are 6.87×10^{-9} and 6.72×10^{-9} mol/cm^2, which are very close to theoretical content (7×10^{-9} mol/cm^2), indicating all the molecular catalysts are almost accessible and electrochemically active on the CNT surface. Moreover, after 30 min chronoamperometric test, the number of electrochemically active sites of CoTMAPc@CNT and CoTAPc@CNT were 6.91×10^{-9} and 6.84×10^{-9} mol/cm^2, which are almost the same as the values before the stability test (Fig. S11b,d). However, for the physically mixed samples, the initial amount of the electrochemically active species of CoTMAPc/CNT and CoTAPc/CNT were only 1.72×10^{-9} and 1.63×10^{-9} mol/cm^2 (Fig. S12a,d). These values were about four times smaller than the

theoretical loading (7×10^{-9} mol/cm^2). The low electrochemical active sites of the physically mixed samples were due to the molecular stacking in physical mixing composites and some initial leaching. Similar to the data in Fig. 1e, the current densities of CoTMAPc/CNT and CoTAPc/CNT also decreased after 30 min stability test (Fig. S12b,e) and the number of electrochemically active site also reduced to 1.48×10^{-9} and 1.01×10^{-9} mol/cm^2, respectively. (Fig. S12c,f). In order to quantify the Co leaching, we further conducted ICP analysis on the post-reaction electrolyte solution at 1 mg/cm^2 catalyst loading. As shown in Table S3, no Co content was detected in the post-reaction electrolyte of CoTAPc@CNT and CoTMAPc@CNT. However, the CoTAPc/CNT and CoTMAPc/CNT showed 11.6 and 43.0 % Co leaching after 30 min electrocatalyst respectively, which was consistent with the current attenuation in Fig. S12 b,e. These results further proved the stability promotion of the covalent bond. The stability of both grafted samples was further evaluated at different applied potentials (Fig. S13). Notably, unlike the rapid attenuation of physically mixed samples, both CoTMAPc@CNT and CoTAPc@CNT have a very stable current density at different potentials for 60 min. The long-term potentiostatic electrolysis of CoTMAPc@CNT was further undertaken at -0.62 V for 12 hours in Fig. 3e. The catalyst achieved a current density of 11.9 mA/cm^2 and a FE_{CO} of 98 % with negligible decay, which amounts to an excellent turnover number (TON) of 373000 over the 12 h electrocatalysis. The excellent stability of CoTMAPc@CNT signifies the effective role of covalent bond in stabilizing the molecular catalysts.

As shown in the LSV curves (Fig. 3a), after covalently grafting on the CNT surface, CoTMAPc@CNT and CoTAPc@CNT presents

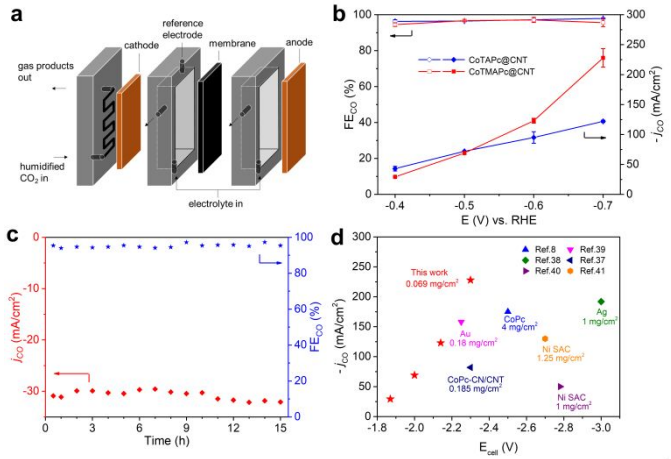

Fig. 4 CO_2RR performance in a flow cell. (a) Graphic illustration of the CO_2 flow cell. (b) Current density and selectivity of CO production at various potentials of CoTAPc@CNT and CoTMAPc@CNT. (c) Long-term electrolysis of CoTMAPc@CNT at -0.4 V vs. RHE. (d) Comparison of the CO_2RR performance of CoTMAPc@CNT to literature data. The catalyst loadings are also listed for comparison.

a low onset potential of -0.28 V and a large total current density of 30.7 mA/cm^2 and 18.4 mA/cm^2 at -0.82 V, respectively. All four samples exhibit similar trends of FE_{CO}, which increase from -0.42 to -0.52 V and keep stable at higher overpotentials (Fig. 3b). The FE_{CO} of CoTMAPc@CNT and CoTAPc@CNT could reach 99 % and 98 % at -0.72 V, while the CoTMAPc/CNT and CoTAPc/CNT only attain 92 % and 90 % at the same potential. Static state measurement shows that CoTMAPc@CNT and CoTAPc@CNT exhibit a high j_{CO} of -21.0 mA/cm^{-2} and -10.9 mA/cm^{-2} at -0.72 V, almost 700% of the CoTMAPc/CNT (-3.1 mA/cm^2) and CoTAPc/CNT (-1.7 mA/cm^2), respectively (Fig. 3c). The ^{1}H NMR spectrum (Fig. S14) shows no liquid products in the post-reaction electrolyte. Two control experiments were conducted: (1) The carbon paper (CP) without deposited catalyst tested in CO_2 saturated 0.5 M $KHCO_3$, and (2) CoTMAPc@CNT with a molecular loading of 7×10^{-9} mol/cm^2 tested in N_2 saturated 0.5 M $KHCO_3$. The CO partial current density (j_{CO}) at different potentials are shown in Table S4. The small j_{CO} confirms that the negligible CO production without CO_2 or with CO_2 but in the absence of catalyst. The reaction kinetics for the CO formation is analyzed by Tafel slope (Fig. 3d). A Tafel slope of 122.6 and 121.4 mV/dec for CoTMAPc@CNT and CoTAPc@CNT indicates no transport limitation and is consistent with the values for a rate-limiting single-electron transfer step.[30]

TOF is defined as the number of reduction products generated per electrocatalytic active site per unit time, representing the intrinsic activity of the catalyst.[35] Here, the TOF values of different samples were calculated from the partial CO current density (Fig. S15) with different molecular catalyst loading (1×10^{-11} to 4×10^{-9} mol/cm^2) at -0.62 V (Fig. 3f). At a loading of 1×10^{-11} mol/cm^2, CoTMAPc@CNT exhibits a maximum TOF_{CO} of 102.9 s^{-1}, far greater than the 68.3 s^{-1} of CoTAPc@CNT, which indicate a higher CO_2RR activity of CoTMAPc molecule. However, the physically mixed samples, CoTMAPc/CNT and CoTAPc/CNT, only show a relatively low TOF_{CO} of 49.3 and 32.8 s^{-1}. In general, the TOFs decrease at higher catalyst loadings, which is because the current densities could be limited by mass transport. When the catalyst loading increases exponentially, TOF_{CO} of CoTMAPc/CNT and CoTAPc/CNT descends much more rapidly to 1.05 and 1.38 s^{-1} at a loading of 4×10^{-9} mol/cm^2, which could result from the molecular catalysts aggregation during electrode preparation and leaching during electrolysis.

The current density of CO_2RR in H-type cells is limited by the slow diffusion and low solubility of CO_2 in aqueous media, which could be resolved by using a flow cell design.[8] Here we further demonstrate that CoTAPc@CNT and CoTMAPc@CNT can deliver commercially relevant current densities in a flow cell configuration. The flow cell was assembled as shown in Fig. 4a. Both the CoTAPc@CNT and CoTMAPc@CNT composites show much higher current densities than those collected in customized three-compartment cell (Fig. S16). The CoTMAPc@CNT shows a high current density of 31.0 mA/cm^2 and FE_{CO} of 94.5 % at a low overpotential of 290 mV (Fig. 4b) with negligible performance decay for 15 h (Fig. 4c). At -0.7 V vs. RHE (η = 590 mV), an outstanding current density of 239 mA/cm^2 and FE_{CO} of 95.6 % was achieved. Salts segregation on the cathode (gas channel) was observed at -0.6 V, which comes from the rapid consumption of water ($CO_2 + 2e^- + H_2O \rightarrow CO + 2OH^-$) and leads to the fluctuation of current density. The excellent CO_2RR activities of CoTMAPc@CNT are comparable to those of other reported catalysts for the conversion of CO_2 to CO (Fig. 4d and Table S5).[8,37-41] For example, compared to other complexes including CoPc, CoPc-CN/CNT and Ni single-atom catalysts (SAC), CoTMAPc@CNT, at a much lower molecular loading of 0.069 mg/cm^2, delivers a much higher current densities than other systems with smaller total cell voltage. Even in comparison to performance of precious metal Au and

silver, the current density and selectivity of CoTMAPc@CNT remains standout.

Conclusions

In conclusion, quaternary ammonium cation can improve the CO_2RR activity of CoPc by decreasing the reaction barriers of intermediate formation and product desorption. However, the enhanced solubility of molecular catalysts due to the charged functional groups hampers the long-term electrolysis and underestimates its function. A strategy for in situ functionalization of immobilized molecular complex on CNT surface is developed by diazo-reaction and methylation reaction. With this design, our cationic catalyst CoTMAPc@CNT achieve a TOF of ~100 s^{-1} at -0.62 V with negligible decay in current density. In a flow cell configuration, it delivers an industrially relevant current density of 239 mA/cm^2 and selectivity of 95.6 % at a cell voltage of 2.3 V and a molecule loading of 0.069 mg/cm^2. This study provides an approach for rational design of molecular catalysts for high-performance CO_2 electroreduction and might have implications for other molecular catalysts in wide applications. It might also call on a revisit of the effect of charged functionalities in heterogeneous molecular electrochemistry.

Experimental

Materials.

All chemicals were used as received without any further treatment. Cobalt phthalocyanine (CoPc, 92%), potassium bicarbonate ($KHCO_3$, 99.5%), iodomethane (CH_3I), 2,6-Lutidine (99 %), isoamyl nitrite and dimethyl sulfoxide (DMSO) were purchased from J&K Scientific LTD. Cobalt tetraamineophthalocyanine (CoTAPc, 95%) was purchased from PorphyChem SAS. Multiwalled carbon nanotube (OD: 10-20 nm L: 5-30 μm) were bought from XFNANO. N, N-Dimethylformamide (DMF), diethyl ether, and ethanol were purchased from LabScan. Deionized water (Millipore Milli-Q grade) with a resistivity of 18.2 MΩ·cm was used in all experiments.

Synthesis of CoTMAPc.

CoTAPc (30 mg, 0.048 mmol) was dissolved in DMF (5 mL) and sonicated for 10 min. Then, 2,6-lutidine (100 μL) and iodomethane (100 μL) was added into the CoTAPc suspension and sonicated for another 10 min. Subsequently, the mixture was stirred at 70 ℃ for 24 h. After the reaction, the solution was poured into diethyl ether (25 mL) and the precipitate was centrifuged and repeatedly washed with diethyl ether and acetone. Finally, the green CoTMAPc product was vacuum dried at 60 °C.

Synthesis of CoTAPc@CNT.

CNT (100 mg) and CoTAPc (34.5 mg, 0.055 mmol) was added into DMSO (50 mL) solution and sonicated for 30 min. The isoamyl nitrite (7.4 μL, 0.055 mmol) was slowly added into DMSO solution under magnetic stirring. Then, the solution was kept at 85 ℃ for 18 h in N_2 atmosphere. After the solution was cooled down to room temperature, the product was collected by centrifugation and washed with DMF and water until the solvent became colorless. Finally, the CoTAPc@CNT composite was vacuum dried at 60 °C.

Synthesis of CoTMAPc@CNT.

CoTAPc@CNT (100 mg) was dispersed in DMF (50 mL). CH_3I (1 mL) and 2,6-lutidine (1 mL) was added and the mixture was stirred at 70 ℃ for 24 h. The final product was collected by centrifugation, washed with DMF (50 mL×3) and DI water (50 mL×3) and vacuum dried.

Material characterization.

The morphology of samples was characterized using transmission electron microscopy (TEM, Philips Technai 12) equipped with energy dispersive X-ray spectroscopy. Zeta-potentials were conducted on Daynamic Light Scattering Particle Size Analyzer (Malvem Zetasizer Nano ZS). Samples were dispersed in DI water and sonicated for 1 h before the test. ICP-atomic emission spectroscopy (ICP-OED) measurements were conducted on Optima 8000 spectrometer. Samples were digested in hot concentrated HNO_3 for 1 h and diluted to desired concentrations. FT-IR spectra were taken on Perkin Elmer Spectrum 100 FT-IR spectrometer. UV-vis spectrum was performed on a Shimadzu 1700 spectrophotometer in DMF solution with a concentration of 1×10^{-5} mol/mL. Raman spectra were collected using a LabRAM HR800 laser confocal micro-Raman spectrometer with a laser wavelength of 514.5 nm. ^1H NMR spectra were recorded at Bruker 600MHz ASCEND AVANCE III HD Nuclear Magnetic Resonance System (NMR-600). The X-ray photoelectron spectroscopy data were collected on a Thermo ESCALAB 250Xi spectrometer equipped with a monochromatic AlK radiation source (1486.6 eV, pass energy 20.0 eV). The data were calibrated with C1s 284.8 eV. Scanning transmission electron microscopy was characterized on a double spherical-aberration-corrected FEI Themis Z microscope at 60 kV.

Working electrode preparation.

The carbon paper (Toray, TGP-H-060, Fuel Cell Store) was punched to discs with a diameter of 0.5 inch. For the CoTMAPc@CNT and CoTAPc@CNT working electrodes preparation, catalyst ink was prepared by dispersing 5 mg of catalyst in 1 mL of DMF with 20 μL 5 wt.% Nafion solution (Sigma Aldrich, Nafion 117, 5 wt.%) and sonicated for 1 h. Then 20 μL of the ink was drop-casted on the carbon paper and subsequently dried naturally overnight. The loading on of the electrode was 75 μg/cm^2 (or 7×10^{-9} mol/cm^2 for molecular catalysts loading). For the preparation of CoPc, CoTAPc and

CoTMAPc working electrodes, 4.5 μmol of molecular catalysts were dispersing in 10 mL DMF with 200 μL Nafion. After sonication, 20 μL catalyst ink was drop-casted on the carbon paper and dried naturally overnight. The catalyst loading is ~ 7×10^{-9} mol/cm^2. For the preparation of physically mixed samples, CoTAPc/CNT and CoTMAPc/CNT, 4.5 μmol of molecular catalysts, 50 mg CNT and 200 μL Nafion were dissolved in DMF and sonicated. Then, 20 μL catalyst ink was dropped on the carbon paper and dried naturally overnight.

Electrochemical measurements.

The electrochemical performance was carried out in a customized three-compartment cell as previously reported.[21,36] A platinum foil and Ag/AgCl leak-free reference (LF-2, Innovative Instrument Inc.) were used as the counter and reference electrode, respectively. The working electrode was separate from the counter electrode by the Nafion-117 membrane (Fuel Cell Store). Before using, the leak-free reference was calibrated as reported.[42] The reference electrode was calibrated with respect to the reversible hydrogen electrode. The calibrations were conducted in high-purity hydrogen-saturated 0.5 M H_2SO_4 electrolyte with a Pt wire as the working and counter electrode at a scan rate of 1 mV/s. The average of the two potentials of each CV curve where the current crossed zero was taken to be the thermodynamic potential. All potentials in this study were converted to the reversible hydrogen electrode (RHE) according to the Nernst equation ($E_{vs.RHE} = E_{vs.Ag/AgCl} + 0.251+0.0592 \times pH$). The 1.75 mL of 0.5 M $KHCO_3$ solution electrolyte was added into the working and counter compartment, respectively. The cell was purged with high-purity CO_2 gas (Linde, 99.999 %, 10 sccm) for 10 min prior to and throughout the duration of all electrochemical measurements. The electrochemical measurements were controlled and recorded with a CHI 650E potentiostat. The automatic iR (95%) compensation was used. The pH values of CO_2 and N_2 saturated 0.5 M $KHCO_3$ electrolyte were 7.25 and 8.36, which was detected by a pH meter (HI 2211, Hanna instruments). Gas-phase products were quantified by an on-line gas chromatograph (Ruimin GC 2060, Shanghai) equipped with a methanizer, a Hayesep-D capillary column, flame ionization detector (FID) for CO and thermal conductivity detector (TCD) for H_2. The CO_2 flow rate was controlled at 10 sccm using a standard series mass flow controller (Alicat Scientific mc-50 sccm). Each run was 8 min long. GC was calibrated using standard mixture gas (Linde) and diluted with nitrogen (Linde 99.999 %).

For flow cell, it contains a gas-diffusion layer (GDL), an anion exchange membrane (Fumasep FAA-3-PK-130), a nickel foam anode and a leak-free Ag/AgCl electrode. The working electrodes were prepared by drop-casting 200 uL of catalyst ink (5 mg/mL) onto the microporous side of the GDL to reach a total mass loading of ~ 1 mg/cm^2, or a molecular loading of ~0.069 mg/cm^2. Prior to electrochemical tests, the electrolytes (1 M KOH, 100 mL) were separately circulated in both the working and counter compartment using peristaltic pumps (Longer, BT100-2J) at a flow rate of 5 mL/min and 100 mL/min, respectively. The CO_2 flow was kept constant at 50 sccm using a mass flow controller. A CHI650E potentiostat was employed to record the electrochemical responses. The electrolyte resistance between reference electrode and working electrode was determined to be approximately 4 Ω using the Potential Electrochemical Impedance Spectroscopy (PEIS) analysis and manually compensated. The gas products were analyzed by an online gas chromatograph.

Computation.

The density functional theoretical (DFT) calculations were carried out with the Gaussian 16.[43] The Becke exchange functional (B) and the Lee–Yang–Parr (LYP) correlation functional within a generalized gradient approximation (GGA) was used to describe the interaction between the ionic cores and electrons.[44,45] The hybrid basic set was employed to optimize all structures and calculate Gibbs free energy. For H, C, N, and O atoms, the basis set b3lyp/6-311+g(d,p) was adopted here. For the metal atom Co, the outer and inner shell valence electrons are described by the effective pseudopotential double-ζ (LANL2DZ) basis set, separately from the core electrons, which were described by the LANL2 effective core potential (ECP). For reaction of CO2RR, the gas-phase errors was corrected as previously reported.[46] For reaction steps involving transfer of a H^+/e^- pair, the free energy of the pair was set as half the free energy of gaseous H_2 ($H^+ + e^- \leftrightarrow 1/2H_2$).[47]

Conflicts of interest

There are no conflicts to declare.

Acknowledgements

This work was supported by the Hong Kong Research Grant Council under Early Career Scheme (Project No. 21300620), Young Scientists Fund of the National Natural Science Foundation of China (Project No. 21905240), and the Program for Professor of Special Appointment (Eastern Scholar) at Shanghai Institutions of Higher Learning and Shanghai Sailing Program (19YF1410600).

References

1 O. S. Bushuyev, P. De Luna, C. T. Dinh, L. Tao, G. Saur, J. van de Lagemaat, S. O. Kelley and E. H. Sargent, *Joule*, 2018, **2**, 825–832.
2 F. P. García de Arquer, C. T. Dinh, A. Ozden, J. Wicks, C. McCallum, A. R. Kirmani, D. H. Nam, C. Gabardo, A. Seifitokaldani, X. Wang, Y. C. Li, F. Li, J. Edwards, L. J. Richter, S. J. Thorpe, D. Sinton and E. H. Sargent, *Science.*, 2020, **367**, 661–666.
3 L. Yoon Suk Lee and K. Y. Wong, *Chem*, 2017, **3**, 717–718.
4 H. Li, C. Qiu, S. Ren, Q. Dong, S. Zhang, F. Zhou, X. Liang, J. Wang, S. Li, M. Yu, *Science.*, 2020, **367**, 667–671.
5 D. Gao, R. M. Arán-Ais, H. S. Jeon and B. Roldan Cuenya, Nat. Catal., 2019, **2**, 198–210.
6 J. Gu, C. S. Hsu, L. Bai, H. M. Chen and X. Hu, *Science.*, 2019, **364**, 1091–1094.

7 D. H. Nam, P. De Luna, A. Rosas-Hernández, A. Thevenon, F. Li, T. Agapie, J. C. Peters, O. Shekhah, M. Eddaoudi and E. H. Sargent, *Nat. Mater.* 2020, **19**, 266–276.
8 S. Ren, D. Joulié, D. Salvatore, K. Torbensen, M. Wang, M. Robert, C. P. Berlinguette, *Science.,* 2019, 365, 367–369.
9 Y. Wu, Z. Jiang, X. Lu, Y. Liang and H. Wang, *Nature*, 2019, **575**, 639–642.
10 F. Li, A. Thevenon, A. Rosas-Hernández, Z. Wang, Y. Li, C. M. Gabardo, A. Ozden, C. T. Dinh, J. Li, Y. Wang, J. P. Edwards, Y. Xu, C. McCallum, L. Tao, Z. Q. Liang, M. Luo, X. Wang, H. Li, C. P. O'Brien, C. S. Tan, D. H. Nam, R. Quintero-Bermudez, T. T. Zhuang, Y. C. Li, Z. Han, R. D. Britt, D. Sinton, T. Agapie, J. C. Peters and E. H. Sargent, *Nature,* 2020, **577**, 509–513.
11 L. Sun, V. Reddu, A. C. Fisher and X. Wang, *Energy Environ. Sci.,* 2020, **13**, 374–403.
12 Y. Q. Zhang, J. Y. Chen, P. E. M. Siegbahn and R. Z. Liao, *ACS Catal*., 2020, **10**, 6332–6345.
13 X. Zhang, Z. Wu, X. Zhang, L. Li, Y. Li, H. Xu, X. Li, X. Yu, Z. Zhang, Y. Liang and H. Wang, *Nat. Commun.*, 2017, 8, 14675.
14 M. Zhu, D. T. Yang, R. Ye, J. Zeng, N. Corbin and K. Manthiram, *Catal. Sci. Technol.*, 2019, **9**, 974–980.
15 M. Wang, K. Torbensen, D. Salvatore, S. Ren, D. Joulié, F. Dumoulin, D. Mendoza, B. Lassalle-Kaiser, U. Işci, C. P. Berlinguette and M. Robert, *Nat. Commun.,* 2019, **10**, 3602
16 S. Zhang, Q. Fan, R. Xia and T. J. Meyer, *Acc. Chem. Res.*, 2020, **53**, 255–264.
17 K. Elouarzaki, V. Kannan, V. Jose, H. S. Sabharwal and J. M. Lee, *Adv. Energy Mater.*, 2019, **9**, 1900090.
18 L. Xie, J. Tian, Y. Ouyang, X. Guo, W. Zhang, U.P. Apfel, W. Zhang and R. Cao, *Angew. Chemie. Int. Ed.*, 2020, DOI: 10.1002/anie.202003836
19 S. Ringe, E. L. Clark, J. Resasco, A. Walton, B. Seger, A. T. Bell and K. Chan, *Energy Environ. Sci.,* 2019, **12,** 3001–3014.
20 J. Choi, J. Kim, P. Wagner, S. Gambhir, R. Jalili, S. Byun, S. Sayyar, Y. M. Lee, D. R. MacFarlane, G. G. Wallace and D. L. Officer, *Energy Environ. Sci.,* 2019, **12**, 747–755.
21 M. Zhu, C. Cao, J. Chen, Y. Sun, R. Ye, J. Xu and Y. F. Han, *ACS Appl. Energy Mater.*, 2019, **2**, 2435–2440.
22 J. Choi, P. Wagner, S. Gambhir, R. Jalili, D. R. Macfarlane, G. G. Wallace and D. L. Officer, *ACS Energy Lett.*, 2019, **4**, 666–672.
23 J. Choi, P. Wagner, R. Jalili, J. Kim, D. R. MacFarlane, G. G. Wallace and D. L. Officer, *Adv. Energy Mater.,* 2018, **8**, 1801280.
24 R. Honna, T. Tsukamoto, T. Shimada, T. Shiragami and S. Takagi, *Clay Science*., 2015, **19**, 53-58.
25 X. Zhang, H. Liu, P. An, Y. Shi, J. Han, Z. Yang, C. Long, J. Guo, S. Zhao, K. Zhao, H. Yin, L. Zheng, B. Zhang, X. Liu, L. Zhang, G. Li and Z. Tang, *Sci. Adv.,* 2020, **6**, eaaz4824.
26 M. M. Bhuyan, H. Okabe, Y. Hidaka and K. Hara, *J. Appl. Polym. Sci.,* 2018, **135**, 45906.
27 R. Asasutjarit, T. Theerachayanan, P. Kewsuwan, S. Veeranodha, A. Fuongfuchat and G. C. Ritthidej, *Aaps Pharmscitech*, 2015, **16**, 1013-1024.
28 S. Liu, H. Bin Yang, S. F. Hung, J. Ding, W. Cai, L. Liu, J. Gao, X. Li, X. Ren, Z. Kuang, Y. Huang, T. Zhang and B. Liu, *Angew. Chemie. Int. Ed.,* 2020, **59**, 798–803.
29 N. Han, Y. Wang, L. Ma, J. Wen, J. Li, H. Zheng, K. Nie, X. Wang, F. Zhao, Y. Li, J. Fan, J. Zhong, T. Wu, D. J. Miller, J. Lu, S. T. Lee and Y. Li, *Chem*, 2017, **3**, 652–664.
30 M. Zhu, R. Ye, K. Jin, N. Lazouski and K. Manthiram, *ACS Energy Lett.*, 2018, **3**, 1381–1386.
31 J. S. Zeng, N. Corbin, K. Williams and K. Manthiram, *ACS Catal.,* 2020, **10**, 4326–4336.
32 N. Li, W. Lu, K. Pei and W. Chen, *RSC Advances*, 2015, **5**, 9374-9380.
33 C. Zhang and J. Zhao, *Int. J. Electrochem. Sci.*, 2017, **12**, 9161–9179.
34 J. Chen, J. Li, W. Liu, X. Ma, J. Xu, M. Zhu and Y. F. Han, *Green Chem.,* 2019, **21**, 6056–6061.
35 M. Zhu, J. Chen, R. Guo, J. Xu, X. Fang and Y. F. Han, *Appl. Catal. B Environ.*, 2019, **251**, 112–118.
36 M. Zhu, J. Chen, L. Huang, R. Ye, J. Xu and Y. F. Han, *Angew. Chemie. Int. Ed.,* 2019, **58**, 6595–6599.
37 X. Lu, Y. Wu, X. Yuan, L. Huang, Z. Wu, J. Xuan, Y. Wang and H. Wang, *ACS Energy Lett.*, 2018, **3**, 2527–2532.
38 R. B. Kutz, Q. Chen, H. Yang, S. D. Sajjad, Z. Liu and I. R. Masel, *Energy Technol.,* 2017, **5**, 929–936.
39 S. Verma, Y. Hamasaki, C. Kim, W. Huang, S. Lu, H. R. M. Jhong, A. A. Gewirth, T. Fujigaya, N. Nakashima and P. J. A. Kenis, *ACS Energy Lett.,* 2018, **3**, 193–198.
40 K. Jiang, S. Siahrostami, T. Zheng, Y. Hu, S. Hwang, E. Stavitski, Y. Peng, J. Dynes, M. Gangisetty, D. Su, K. Attenkofer and H. Wang, *Energy Environ. Sci.,* 2018, **11**, 893–903.
41 T. Zheng, K. Jiang, N. Ta, Y. Hu, J. Zeng, J. Liu and H. Wang, *Joule*, 2019, **3**, 265–278.
42 R. Ye, Z. Peng, T. Wang, Y. Xu, J. Zhang, Y. Li, L. G. Nilewski, J. Lin and J. M. Tour, *ACS Nano,* 2015, **9**, 9244–9251.
43 M. J. Frisch, G. W. Trucks, H. B. Schlegel, G. E. Scuseria, M. A. Robb, J. R. Cheeseman, G. Scalmani, V. Barone, G. A. Petersson, H. Nakatsuji, X. Li, M. Caricato, A. V. Marenich, J. Bloino, B. G. Janesko, R. Gomperts, B. Mennucci, H. P. Hratchian, J. V. Ortiz, A. F. Izmaylov, J. L. Sonnenberg, D. Williams-Young, F. Ding, F. Lipparini, F. Egidi, J. Goings, B. Peng, A. Petrone, T. Henderson, D. Ranasinghe, V. G. Zakrzewski, J. Gao, N. Rega, G. Zheng, W. Liang, M. Hada, M. Ehara, K. Toyota, R. Fukuda, J. Hasegawa, M. Ishida, T. Nakajima, Y. Honda, O. Kitao, H. Nakai, T. Vreven, K. Throssell, J. A. Montgomery, Jr., J. E. Peralta, F. Ogliaro, M. J. Bearpark, J. J. Heyd, E. N. Brothers, K. N. Kudin, V. N. Staroverov, T. A. Keith, R. Kobayashi, J. Normand, K. Raghavachari, A. P. Rendell, J. C. Burant, S. S. Iyengar, J. Tomasi, M. Cossi, J. M. Millam, M. Klene, C. Adamo, R. Cammi, J. W. Ochterski, R. L. Martin, K. Morokuma, O. Farkas, J. B. Foresman and D. J. Fox, Gaussian, Inc., *Wallingford CT*, 2016.
44 B. Delley, *J. Chem. Phys.,* 2000, **113**, 7756–7764.
45 B. Delley, *J. Chem. Phys.,* 1990, **92**, 508–517.
46 F. Calle-Vallejo and M. T. M. Koper, *Angew. Chemie. Int. Ed.*, 2013, **52**, 7282–7285.
47 A. A. Peterson, F. Abild-Pedersen, F. Studt, J. Rossmeisl and J. K. Nørskov, *Energy Environ. Sci.*, 2010, **3**, 1311–1315.